Supporting Information

Regulation of biomolecular motor-driven cargo transport by microtubules under mechanical stress

Syeda Rubaiya Nasrin,[†,‖] Tanjina Afrin,[†,‖] Arif Md. Rashedul Kabir,[‡] Daisuke Inoue,[‡] Takayuki Torisawa,[⊥,□] Kazuhiro Oiwa,[§] Kazuki Sada,[‖,‡] and Akira Kakugo *,[‖,‡]

[‖] Graduate School of Chemical Sciences and Engineering, Hokkaido University, Sapporo 060-0810, Hokkaido, Japan.

[‡]Faculty of Science, Hokkaido University, Sapporo 060-0810, Hokkaido, Japan.

[⊥]Cell Architecture Laboratory, Structural Biology Center, National Institute of Genetics, Mishima 411-8540, Japan.

[□]Department of Genetics, SOKENDAI (The Graduate University for Advanced Studies), Mishima 411-8540, Japan.

[§]Advanced ICT Research Institute, National Institute of Information and Communications Technology, Kobe, Hyogo 651-2492, Japan.

[†]These authors contributed equally to this work.

*Corresponding author: kakugo@sci.hokudai.ac.jp

SUPPORTING FIGURES	**:**	Figures S1- S9
SUPPORTING INFORMATION	**:**	I
SUPPORTING TABLES	**:**	Tables S1- S7

Figure S1

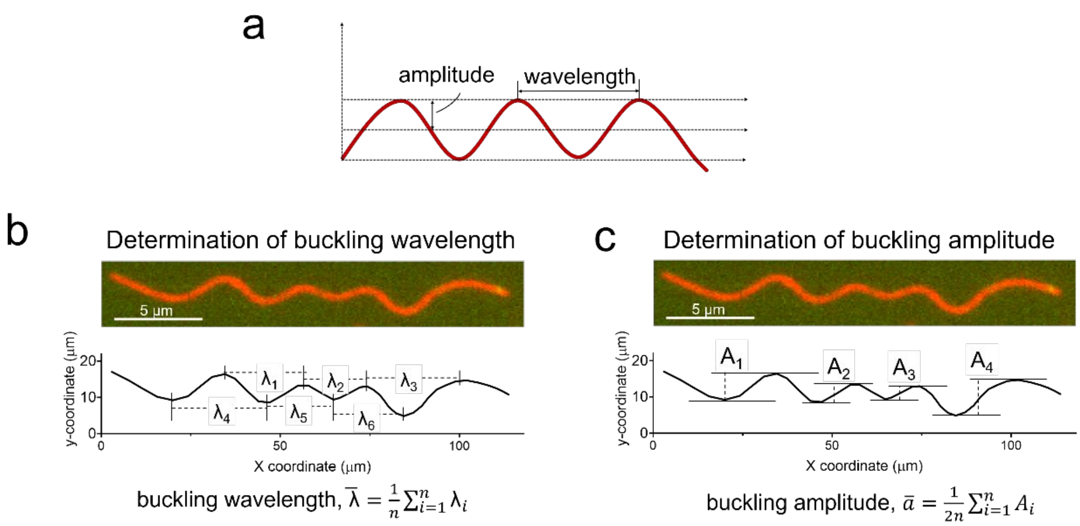

a. Definition of buckling amplitude and buckling wavelength of a buckled MT with a uniform sinusoidal wave shape. b. Determination of buckling wavelength of a buckled MT under applied compressive strain of 10.0 % (top). For each buckling crest and trough of the buckled MTs the wavelengths are measured and the mean wavelength is calculated for MTs buckled under a particular compressive strain (bottom). c. Determination of buckling amplitude of a buckled MT under applied compressive strain of 10.0 % (top). For each buckling crest and trough of the buckled MTs the amplitudes are measured and the mean amplitude is calculated for MTs buckled under a particular compressive strain (bottom).

Figure S2

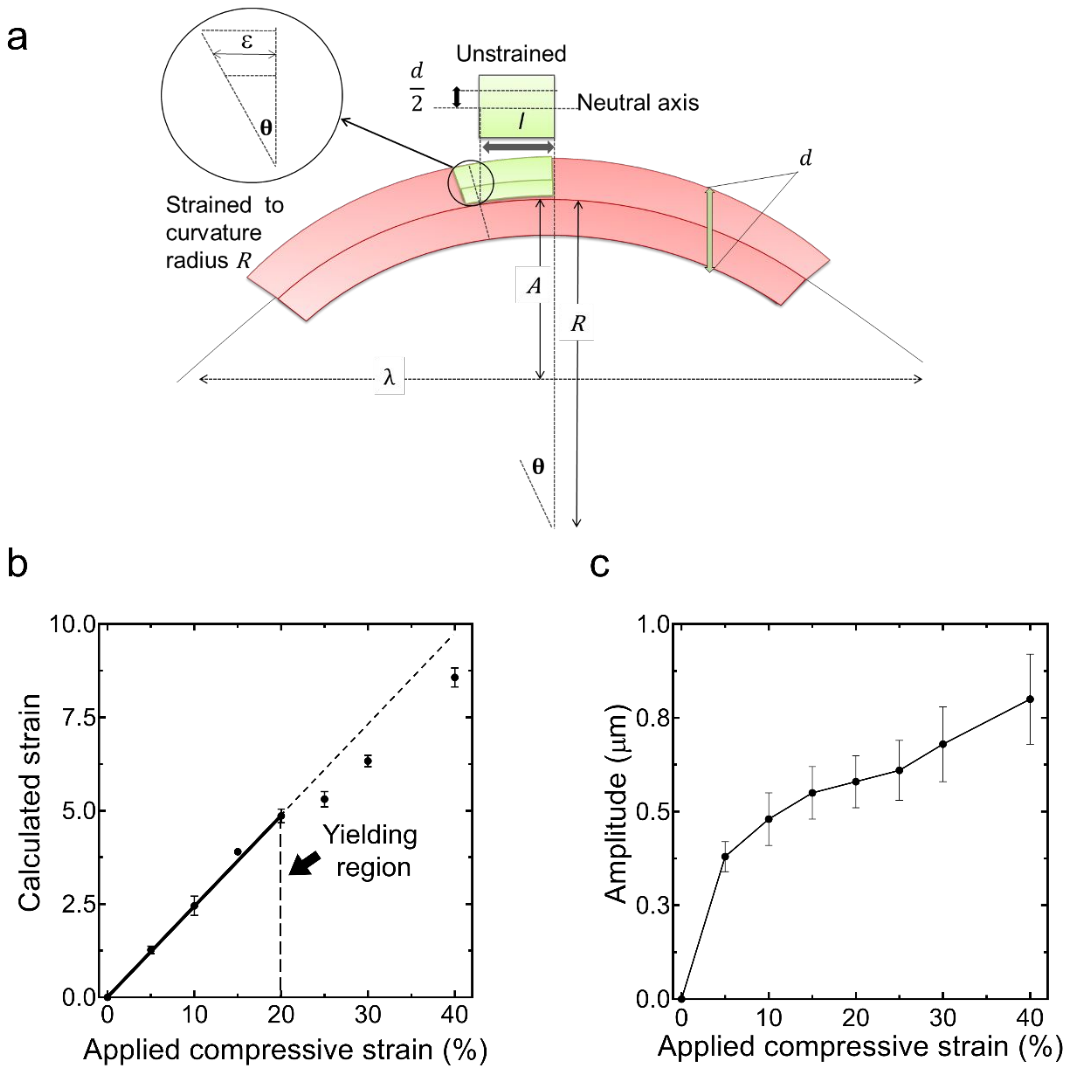

a. Schematic illustration of the curvature of a beam under compression, which is resembled by the buckling of an MT under compressive stress and can be applied to determine the calculated maximum strain experienced by the MT. The calculated maximum strain, ε can be expressed by the equation: $\varepsilon = (\frac{2\pi}{\lambda})^2 A \frac{d}{2}$; where, λ = wavelength, A = amplitude, d = diameter of the cross-section of MT, and R = radius of curvature. The calculated maximum strain is a dimensionless quantity. **b.** Relationship between calculated maximum strain at MT with applied compressive strain. The relation between applied and calculated compressive strains was linear up to 20.0% applied strain, above which deviation from linearity could be observed. Therefore, the yielding region of the MT deformation may have started from the 20.0% strain. **c.** The change in amplitude of the waves caused by the buckling of MTs at different applied compressive strains. Error bar: standard error.

Figure S3

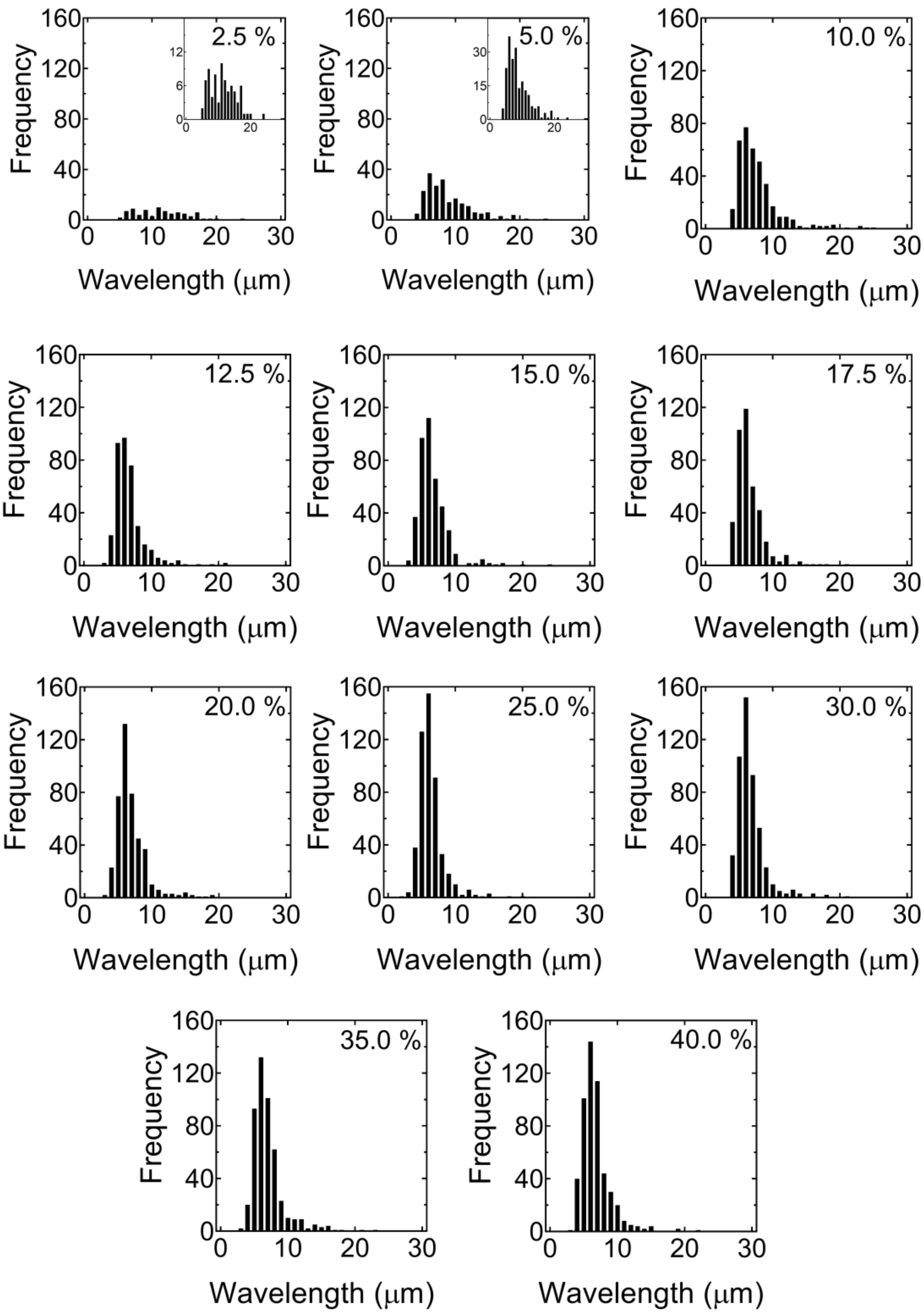

The distributions of frequencies of buckling wavelengths of the buckled MTs at different applied compressive strains. The applied compressive strain on the MTs in each case is mentioned in the legend. The buckling wavelength frequency distributions of MTs under 2.5 % and 5.0 % compressive strains are shown in insets. Number of events analyzed are 80, 207, 365, 370, 413, 402, 429, 492, 493, 479, and 520 buckling crests of MTs created under 2.5, 5.0, 10.0, 12.5, 15.0, 17.5, 20.0, 25.0, 30.0, 35.0 and 40.0% compressive strains respectively.

Figure S4

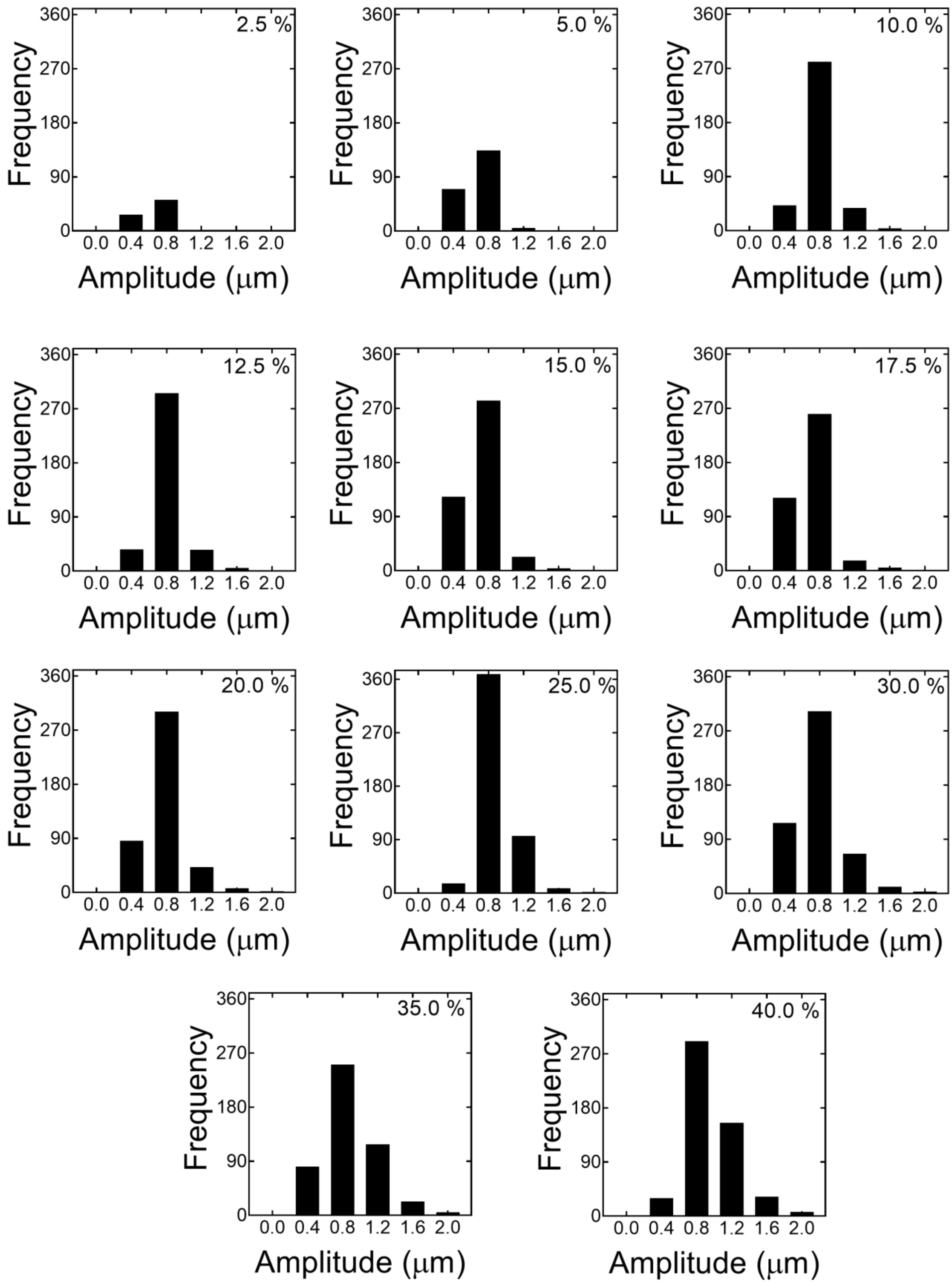

The distributions of frequencies of buckling amplitudes of the buckled MTs at different applied compressive strains. The applied compressive strain on the MTs in each case is mentioned in the legend. Number of events analyzed are same as given in Figure S3.

Figure S5

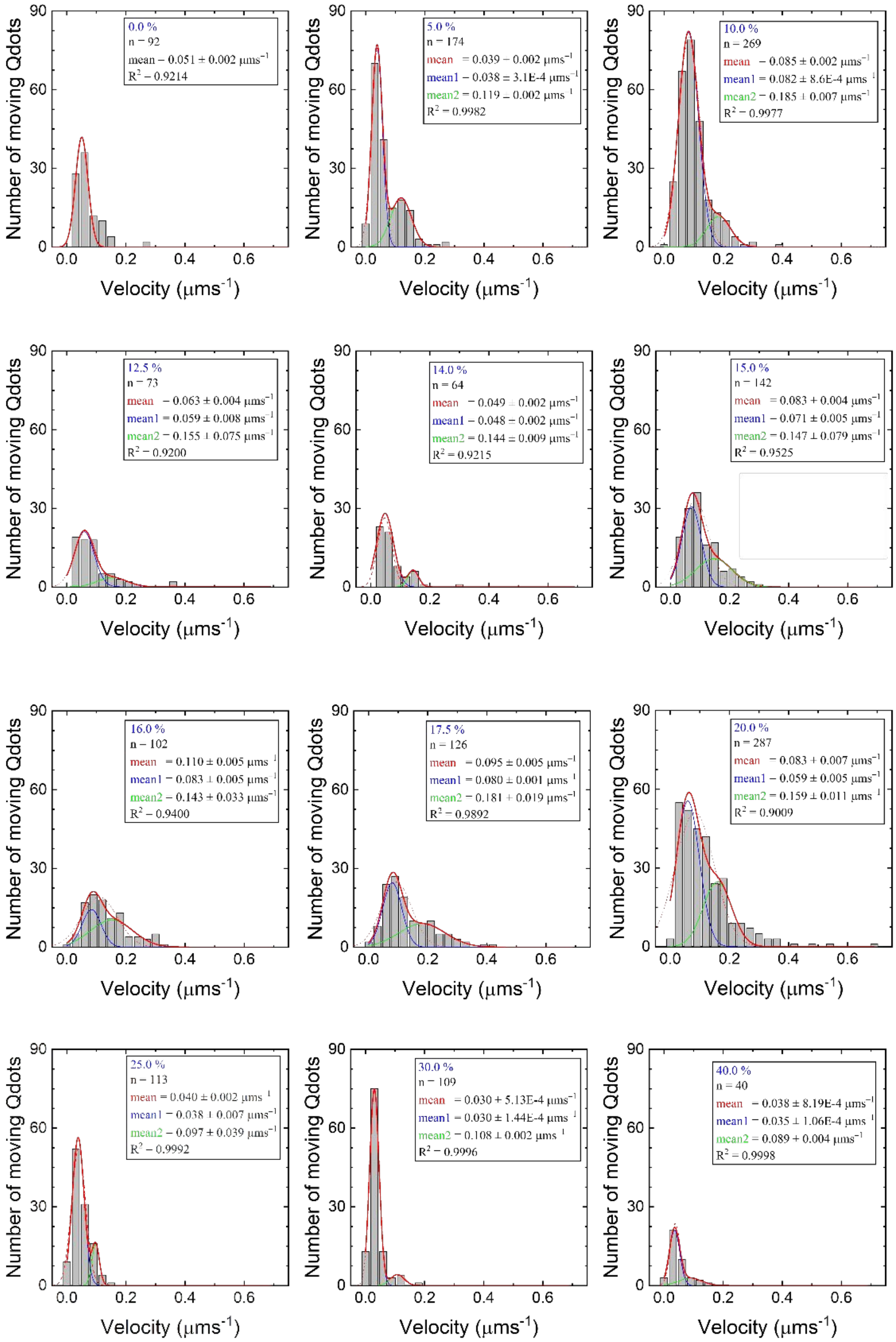

Distribution of velocities of dynein driven Qdots along MTs under different compressive strains. For the cases of the deformed MTs, the distributions showed two peaks. Therefore, the distributions were fitted to

2-peak Gaussian distribution using equation, $y = y_o + \frac{A_1}{w_1\sqrt{\frac{\pi}{2}}}e^{-2\frac{(x-x_{c1})^2}{w_1{}^2}} + \frac{A_2}{w_2\sqrt{\frac{\pi}{2}}}e^{-2\frac{(x-x_{c2})^2}{w_2{}^2}}$, where A, w, and x_c are areas, widths, and centers of the peaks 1 and 2 with a shared y-offset equal to zero (0), respectively. The solid red line is the convoluted peak from the first and second peaks represented using the blue and green solid lines, respectively. Bin size = 0.03 μms^{-1}. Number of events analyzed, mean velocities and goodness of fit are mentioned in respective plots. "mean1" and "mean2" correspond to the means of the two peaks that were obtained from the multiple peak curve fitting whereas, "mean" in each plot represents the mean velocity obtained from single peak Gaussian fittings of the distributions (red dashed lines). The deviations of the mean values are standard errors. The two populations moving with slow and fast velocities, as found from the velocity distributions, are considered to arise from Qdot transport by one and two dyneins, respectively.

Figure S6

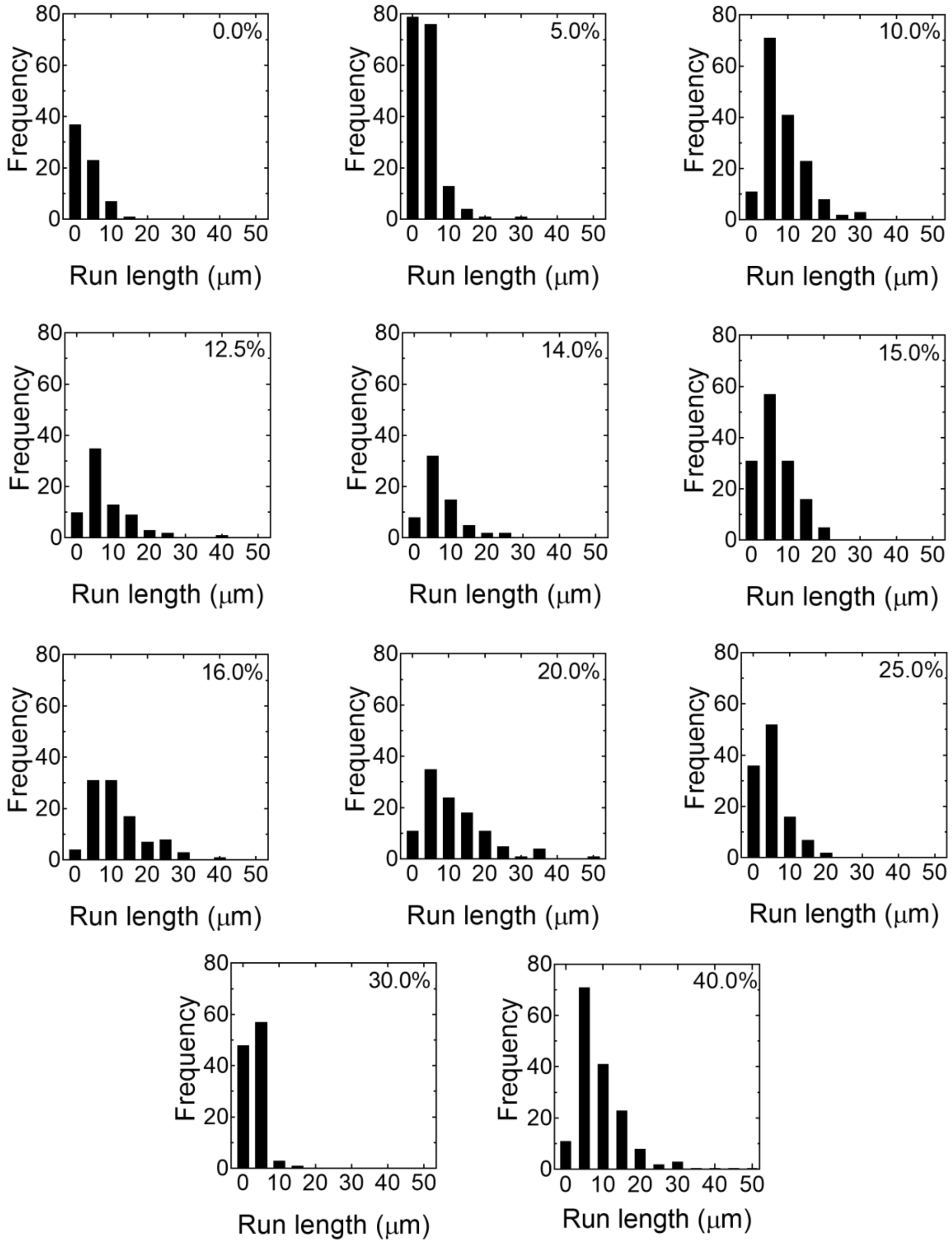

Distribution of percent frequency of run lengths of the Qdot-dynein conjugates along buckled MTs at different applied compressive strains. The applied compressive strains are provided in the legends. Bin size to obtain this distribution was 3.0 μm. The number of events considered in each case is the same as in Figure S5.

Figure S7

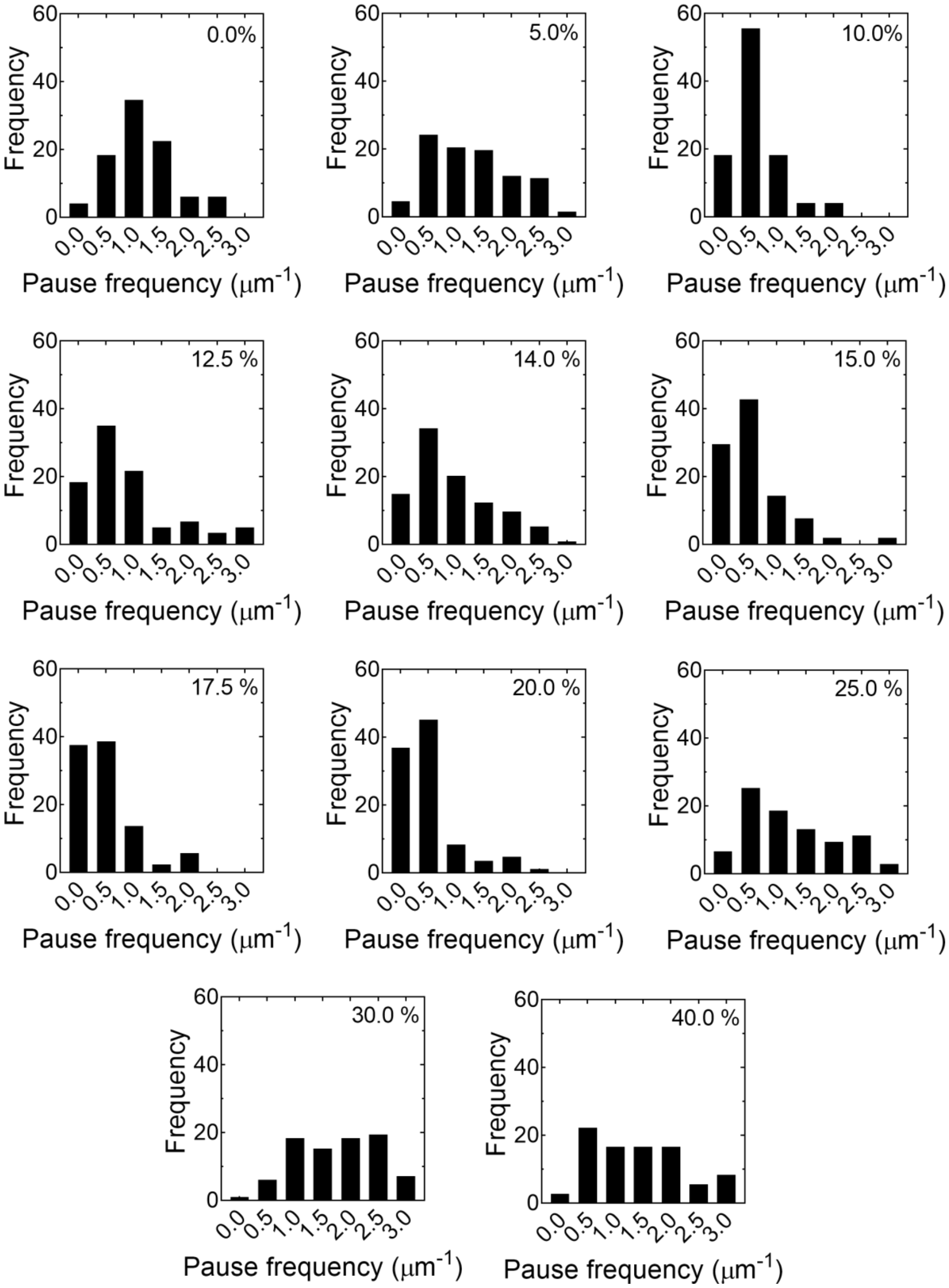

Distribution of percent frequency of pause frequencies (pause per unit length) of the Qdot-dynein conjugates moving along buckled MTs at different applied compressive strains. The applied compressive strains are provided in the legends. Bin size to obtain this distribution was 0.5 μm^{-1}. The number of events considered are 68, 174, 109, 73, 129, 139, 102, 126, 110, 113, 109, and 40 along MTs under 2.5, 5.0, 10.0, 12.5, 15.0, 17.5, 20.0, 25.0, 30.0, 35.0 and 40.0% compressive strains respectively . Qdots that showed no pause while being transported, i.e. with pause frequency = 0.0, are not included in the histograms.

Figure S8

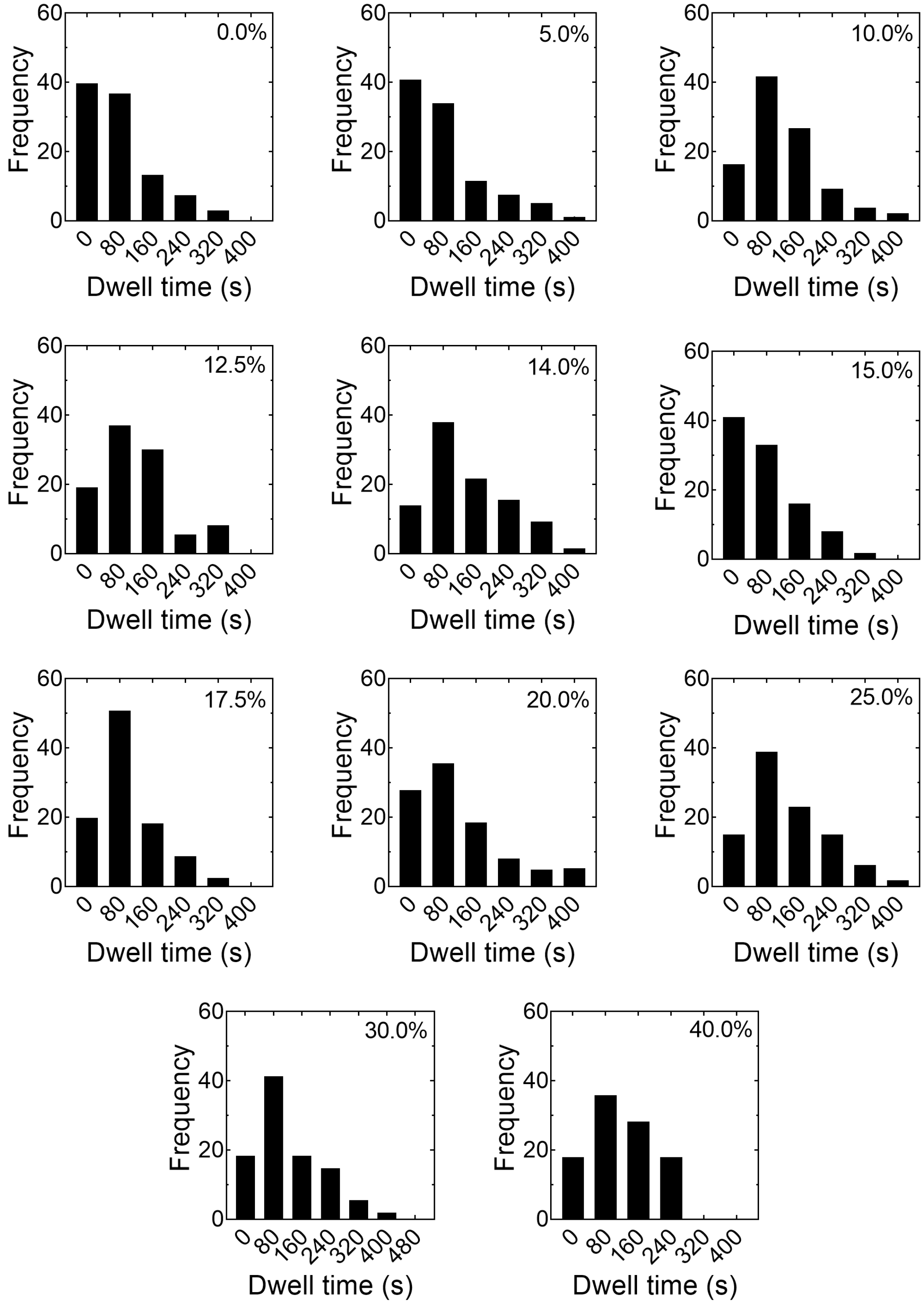

Distribution of percent frequency of dwell times of the Qdot-dynein conjugates moving along buckled MTs at different applied compressive strains. The applied compressive strains are provided in the legends. Bin size to obtain this distribution was 80 s. The number of events considered are the same as mentioned in Figure S5.

Figure S9

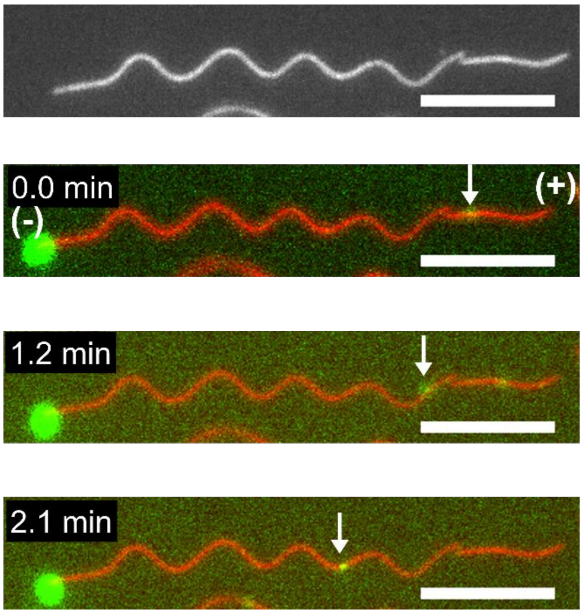

Fluorescence microscopy image of a buckled MT under 40.0 % compressive strain (top). Time-lapse fluorescence microscopy images showing the transport of Qdot conjugated with dyneins along the compression induced- broken MT. Scale bar: 10 µm.

I. Determination of calculated maximum strain at buckled MTs

The buckled MT is considered as a hollow beam where the beam is bent to a (uniform) radius of curvature, *R*. Considering a section of unit length (unstrained) as shown in Figure S1, the angle θ (~tan θ) ≈ *1/R* after bending.

From the two similar triangles in the diagram, θ is also given by the surface strain ε divided by *r*, the radius of the pole, $\theta = \frac{\varepsilon}{d/2}$.

The surface strain, ε, is thus given by the ratio *r* / *R*. This strain is compressive on the "inside" surface of the pole and tensile on the "outside" surface. The stresses induced by such bending can be high. The axial stress, σ, is given by the product of Young's modulus, *E*, and strain, ε. $\sigma = E\,\varepsilon = E\,r\,/\,R$

$$\text{We obtain, } \theta = \frac{1}{R} = \frac{\varepsilon}{d/2};$$

$$\Rightarrow \varepsilon = \frac{1}{R}.\frac{d}{2};$$

The relationship of the radius of curvature (R) of a buckled MT with the buckling wavelength (λ) and amplitude (A) is given by, $R = \frac{1}{k^2 A} = \frac{1}{\left(\frac{2\pi}{\lambda}\right)^2 A}$; … … … (1)

[where, wave number, k = $\frac{2\pi}{\lambda}$]

$$\therefore \varepsilon = \left(\frac{2\pi}{\lambda}\right)^2 A \frac{d}{2} \text{ … … … (2)}$$

Therefore, with the amplitude and wavelengths known, the calculated maximum strain applied on the MTs can be determined from the above equation.

Table S1. Results of the normality test of the velocities of Qdots transported by dyneins

Normality tests determine if the distribution of the mean velocities of the Qdots transported by multiple dyneins along MTs under different compressive stresses (data of Figure S5) are normally distributed at alpha =0.0001. Almost all data were non-normally distributed.

D'Agostino & Pearson test				
% Strain	K2	P-value	Passed normality test ?	P-value summary
0.0	54.9	<0.0001	No	****
5.0	55.46	<0.0001	No	****
10.0	90.05	<0.0001	No	****
12.5	44.58	<0.0001	No	****
14.0	41.59	<0.0001	No	****
15.0	70.22	<0.0001	No	****
16.0	9.077	0.0107	Yes	*
17.5	22.95	<0.0001	No	****
20.0	147.6	<0.0001	No	****
25.0	14.71	0.0006	No	***
30.0	81.08	<0.0001	No	****
40.0	15.86	0.0004	No	***

Table S2. Statistical analysis of velocities of dynein-driven Qdot transport along the MTs under applied compressive strain.

Kruskal-Wallis test followed by *Dunn*'s multiple comparison test was used to compare among the velocities of dynein based Qdot transport along MTs under different compressive strains (data in Figure S5). Summarized results are shown in Figure 4a.

Kruskal-Wallis test	
P value	<0.0001
Do the medians vary significantly?	Yes
Number of groups	12
Kruskal-Wallis statistic	426.8
Data summary	
Number of treatments (columns)	12
Number of values (total)	1591

Alpha	0.0001		
Dunn's multiple comparisons tests	Mean rank diff.	Summary	Adjusted P-Value
0.0 % vs. 15.0 %	-447.6	****	<0.0001
0.0 % vs. 16.0 %	-610.4	****	<0.0001
0.0 % vs. 17.5 %	-580.8	****	<0.0001
0.0 % vs. 20.0 %	-462.1	****	<0.0001
5.0 % vs. 10.0 %	-319.3	****	<0.0001
5.0 % vs. 15.0 %	-312.7	****	<0.0001
5.0 % vs. 16.0 %	-475.5	****	<0.0001
5.0 % vs. 17.5 %	-445.9	****	<0.0001
5.0 % vs. 20.0 %	-327.2	****	<0.0001
10.0 % vs. 14.0 %	243.5	****	<0.0001
12.5 % vs. 30.0 %	488.5	****	<0.0001
14.0 % vs. 20.0 %	-251.4	****	<0.0001
14.0 % vs. 30.0 %	413.7	****	<0.0001
15.0 % vs. 25.0 %	484.0	****	<0.0001
15.0 % vs. 30.0 %	650.6	****	<0.0001
15.0 % vs. 40.0 %	513.7	****	<0.0001
20.0 % vs. 25.0 %	498.5	****	<0.0001

20.0 % vs. 30.0 %	665.1	****	<0.0001
20.0 % vs. 40.0 %	528.2	****	<0.0001

Table S3. Results of the normality test of run lengths of Qdots transported by dyneins

Normality tests determine if the distribution of the run lengths of the Qdots transported by multiple dyneins along MTs under different compressive stresses (data of Figure S7) are normally distributed at alpha =0.001. Almost all data were non-normally distributed.

D'Agostino & Pearson test				
% Strain	K2	P-value	Passed normality test ?	P-value summary
0.0	28.99	<0.0001	No	****
5.0	146.5	<0.0001	No	****
10.0	39.47	<0.0001	No	****
12.5	40.63	<0.0001	No	****
14.0	22.53	<0.0001	No	****
15.0	14.46	<0.0001	No	****
16.0	19.06	<0.0001	No	****
17.5	42.79	<0.0001	No	****
20.0	39.44	<0.0001	No	****
25.0	28.54	<0.0001	No	****
30.0	51.59	<0.0001	No	****
40.0	55.16	<0.0001	No	****

Table S4. Statistical analysis of run lengths of dynein-driven Qdot transport along the MTs under applied compressive strain.

Kruskal-Wallis test followed by *Dunn*'s multiple comparison test was used to compare among the velocities of dynein based Qdot transport along MTs under different compressive strains (data in Figure S6). Summarized results are shown in Figure 3a.

Kruskal-Wallis test	
P value	<0.0001
Do the medians vary significantly?	Yes
Number of groups	12
Kruskal-Wallis statistic	347.5
Data summary	
Number of treatments (columns)	12
Number of values (total)	1591

Alpha	0.0001		
Dunn's multiple comparisons tests	Mean rank diff.	Summary	Adjusted P-Value
0.0 % vs. 10.0 %	-470.2	****	<0.0001
0.0 % vs. 15.0 %	-319.9	****	<0.0001
0.0 % vs. 20.0 %	-501.6	****	<0.0001
5.0 % vs. 10.0 %	-397.5	****	<0.0001
5.0 % vs. 15.0 %	-247.2	****	<0.0001
5.0 % vs. 16.0 %	-493.2	****	<0.0001
5.0 % vs. 17.5 %	-422.4	****	<0.0001
5.0 % vs. 20.0 %	-428.9	****	<0.0001
10.0 % vs. 25.0 %	265.5	****	<0.0001
10.0 % vs. 30.0 %	449.9	****	<0.0001
10.0 % vs. 40.0 %	335.2	****	<0.0001
17.5 % vs. 25.0 %	290.4	****	<0.0001
17.5 % vs. 30.0 %	474.8	****	<0.0001
17.5 % vs. 40.0 %	360.2	****	<0.0001
20.0 % vs. 25.0 %	297.0	****	<0.0001
20.0 % vs. 30.0 %	481.3	****	<0.0001
20.0 % vs. 40.0 %	366.7	****	<0.0001

Table S5. Results of the normality test of pause frequencies of Qdots transported by dyneins

Normality tests determine if the distribution of the run lengths of the Qdots transported by multiple dyneins along MTs under different compressive stresses (data of Figure S7) are normally distributed at alpha =0.0001. Almost all the data were non-normally distributed.

D'Agostino & Pearson test				
% Strain	K2	P-value	Passed normality test ?	P-value summary
0.0	46.43	<0.0001	No	****
5.0	62.64	<0.0001	No	****
10.0	41.58	<0.0001	No	****
12.5	24.4	<0.0001	No	****
14.0	48.27	<0.0001	No	****
15.0	95.84	<0.0001	No	****
16.0	102.9	<0.0001	No	****
17.5	96.57	<0.0001	No	****
20.0	45.13	<0.0001	No	****
25.0	17.52	0.0002	Yes	***
30.0	5.821	0.0544	Yes	ns
40.0	16.54	0.0003	Yes	***

Table S6. Statistical analysis of pause frequencies of dynein-driven Qdot transport along the MTs under applied compressive strain

Kruskal-Wallis test followed by *Dunn*'s multiple comparison test was used to compare among the pause frequencies of dynein based Qdot transport along MTs under different compressive strains (data in Figure S7). Summarized results are shown in Figure 3b.

Kruskal-Wallis test	
P value	<0.0001
Do the medians vary significantly?	Yes
Number of groups	12
Kruskal-Wallis statistic	136.4
Data summary	
Number of treatments (columns)	12
Number of values (total)	1292

Alpha	0.0001		
Dunn's multiple comparisons tests	Mean rank diff.	Summary	Adjusted P-Value
0.0 % vs. 25.0 %	-314.6	****	<0.0001
0.0 % vs. 30.0 %	-300.5	****	<0.0001
15.0 % vs. 25.0 %	-374.5	****	<0.0001
15.0 % vs. 30.0 %	-360.4	****	<0.0001
15.0 % vs. 40.0 %	-330.2	***	0.0002
17.5 % vs. 25.0 %	-313.7	****	<0.0001
17.5 % vs. 30.0 %	-299.6	****	<0.0001
17.5 % vs. 40.0%	-269.4	*	0.0107
20.0 % vs. 25.0 %	-285	****	<0.0001
20.0 % vs. 30.0 %	-270.9	****	<0.0001
20.0 % vs. 40.0 %	-240.7	ns	0.0618
25.0 % vs. 30.0 %	14.12	ns	>0.9999
25.0 % vs. 40.0 %	44.28	ns	>0.9999
30.0% vs. 40.0 %	30.17	ns	>0.9999

Table S7. Statistical analysis of dwell times of dynein-driven Qdot transport along the MTs under applied compressive strain

Kruskal-Wallis test followed by *Dunn*'s multiple comparison test was used to compare among the dwell times of dynein based Qdot transport along MTs under different compressive strains (data in Figure S8). Summarized results are shown in Figure 3c.

Kruskal-Wallis test	
P value	<0.0001
Do the medians vary significantly?	Yes
Number of groups	12
Kruskal-Wallis statistic	55.23
Data summary	
Number of treatments (columns)	12
Number of values (total)	1591

Alpha	0.0001		
Dunn's multiple comparisons tests	Mean rank diff.	Summary	Adjusted P-Value
0.0 % vs. 5.0 %	34.12	ns	>0.9999
0.0 % vs. 10.0 %	-164.4	ns	0.1175
0.0 % vs. 12.5 %	-142.2	ns	0.8023
0.0 % vs. 14.0 %	-259.3	**	0.0028
0.0 % vs. 15.0 %	-24.24	ns	>0.9999
0.0 % vs. 16.0 %	-155.1	ns	0.3924
0.0 % vs. 17.5 %	-71.16	ns	>0.9999
0.0 % vs. 20.0 %	-96.78	ns	>0.9999
0.0 % vs. 25.0 %	-238.3	*	0.0113
0.0 % vs. 30.0 %	-177.2	ns	0.1682
0.0 % vs. 40.0 %	-178.7	ns	0.6318